Growth of Carbon Nanocoils from K and Ag Cooperative Bicatalyst Assisted Thermal Decomposition of Acetylene

Wen-Chih Liu,[†] Huang-Kai Lin,[†] Yu-Liang Chen,[†] Chi-Young Lee,[‡] and Hsin-Tien Chiu[†,*]

[†]Department of Applied Chemistry, National Chiao Tung University, Hsinchu, Taiwan, 30050, R.O.C and [‡]Department of Materials Science and Engineering and Center for Nanotechnology, Materials Science, and Microsystems, National Tsing Hua University, Hsinchu, Taiwan, 30043, R.O.C

ABSTRACT Growth of amorphous carbon nanocoil (CNC) from acetylene on Si substrates was achieved by using nanosized Ag and K as the catalysts. The deposition of CNC was carried out inside a hot-wall reactor at 723 K using H_2 as the carrier gas. Based on the observed results, we propose a cooperative bimetal catalyst enhanced vapor−liquid−solid (VLS) growth mechanism to rationalize the CNC growth. In the reaction, the liquid phase metallic K dehydrogenated acetylene into the solid-state carbon, while the Ag nanoparticle assisted the extension of carbon one-dimensionally (1-D) *via* a tip-growth mechanism. Due to the adhesive force between the K liquid and the carbon, the 1-D solid curled along the C−K interface into the nanocoil shape. Some CNC samples were further heat-treated at 1423 K and showed very good field emission properties. They emitted electrons (10 μA/cm^2) at a turn-on field E_{to} of 2.51 V/μm, while J_{max} reached 17.71 mA/cm^2 at 5.64 V/μm. The field enhancement factor β was calculated to be 2124, comparable to other carbon nanotube (CNT) and CNC based emitters. The CNC was also characterized by using the electrochemical behavior of $K_3[Fe(CN)_6]$ *via* cyclic voltammetry (CV). The electrochemical surface area of a CNC electrode (geometric surface area 0.078 cm^2) was calculated to be 0.143 cm^2. These properties suggest that the CNC electrodes may have potential applications in field emission and electrochemical devices.

KEYWORDS: carbon nanocoils · vapor−liquid−solid growth · K catalyst · Ag catalyst · field emission · electrochemical surface area

After the discovery of carbon nanotubes (CNTs) by Iijima,[1] many new types of carbon nanomaterials have been discovered. One of them, carbon nanocoils (NCs), has attracted considerable attention.[2−6] Because of their unique morphology and physical properties, carbon NCs (CNCs) have been proposed for potential applications in microwave absorbers, field emission displays, and structural foams for cushioning and energy dissipation.[7−13] CNCs were generally prepared by chemical vapor deposition (CVD) employing metal nanoparticles (NPs) as the catalysts for vapor−liquid−solid (VLS) types of growth. Examples of various fabrication methods of CNCs and carbon microcoils (CMCs) are summarized in Table S1 in the Supporting Information. Most of the processes can mass produce high-quality coiled carbon materials controllably. Although many hydrocarbons were used as the sources for carbon deposition, acetylene was applied more often in many cases. Many nanosized metal catalysts, such as Fe, Co, and Ni, commonly employed to fabricate straight carbon materials, were also used to grow coiled carbons.[14−16] For example, Motojima *et al.* deposited CMCs from acetylene and propane in the presence of thiophene on micrometer-sized Ni particles at 1043 K.[17] Bajpai *et al.* synthesized aligned helical CNT arrays on quartz by copyrolysis of $Fe(CO)_5$ and pyridine at 1173−1373 K.[5] Several groups grew CNCs successfully from acetylene at temperatures above 973 K using catalysts containing both transition metal Fe and main group metal Sn or In.[18] In an interesting example, Qin *et al.* reported that CNCs could be grown at a temperature as low as 468 K using Cu NPs as the catalyst.[4] Even though the cases were plentiful, their growth mechanisms are yet to be fully understood. Motojima *et al.* proposed that three-dimensional growth of carbon fibers from different crystalline faces of a Ni catalyst particle caused the formation of CMCs.[19] On the other hand, Amelinckx *et al.* suggested the concept of a spatial-velocity hodograph that nonuniformity of carbon extrusion speed at different parts of a catalyst grain leads to the helical growth.[20,21] In addition, it was proposed by Bandaru *et al.* that repulsive interactions at the interface between the growing carbon nanostructure and the nonwetting catalyst particle might promote nonlinear growths.[22] Nevertheless, none of the above-mentioned models have been proved experimentally.

Previously, we reported that highly reactive alkali metals such as Na can be employed to synthesize carbon nanomaterials *via* stoichiometric dechlorination of

*Address correspondence to htchiu@faculty.nctu.edu.tw.

Received for review August 10, 2009 and accepted June 01, 2010.

Published online June 8, 2010.
10.1021/nn901926r

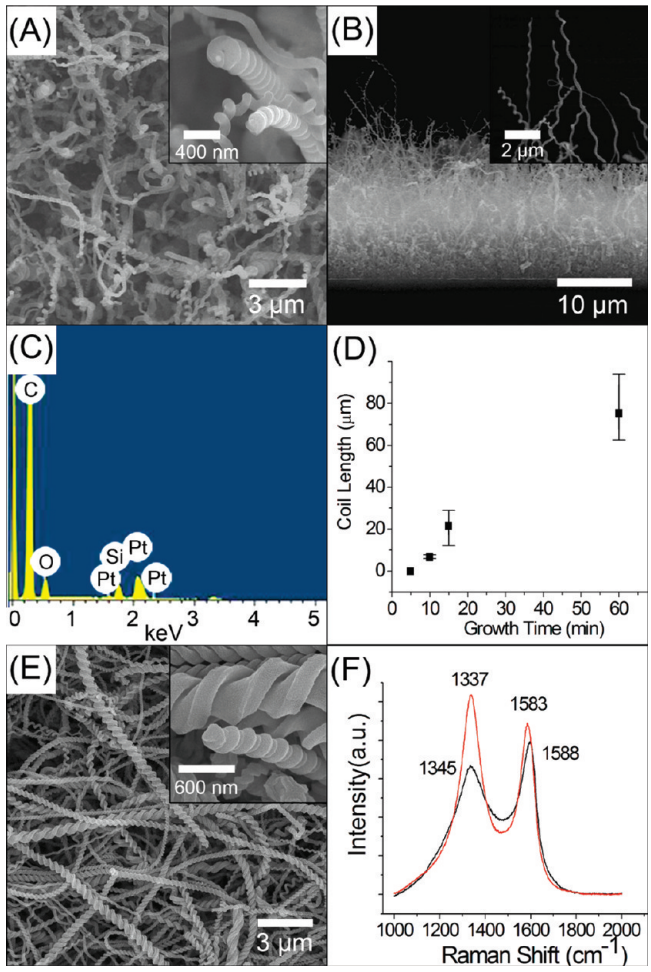

Figure 1. SEM images of as-grown CNCs: (A) low and high (inset) magnification top views and (B) low and high (inset) magnification side views. (C) EDS of as-grown CNCs after being washed with DI water. The signals of O, Si, and Pt atoms are from the surface oxidation, the substrate, and the sputtered conductive layer, respectively. (D) Distribution of lengths (the bars) of 50 CNCs at various growth times. The averaged lengths are shown as the squares. (E) Low and high (inset) magnification SEM images of annealed CNCs. (F) Raman spectra of as-grown (black) and annealed (red) CNCs.

hexachlorobenzene.[23] On the other hand, as shown in Table S1 in the Supporting Information, acetylene is frequently employed to grow coiled carbon materials. Acetylene has a high positive enthalpy of formation ΔH_f°, 226.7 kJ/mol.[24] As a result, the molecule is the least thermodynamically stable two-carbon organic molecule to exist at room temperature. However, the kinetic barrier to decompose acetylene into its elemental form is still high because of its high bond dissociation energy (BDE), 523 kJ/mol.[25] For example, acetylene black, a common carbon material, can be produced by thermolysis of acetylene, but only at temperatures above 1073 K.[26] We have discovered that, by employing metallic Na as a dehydrogenation catalyst, the energy barrier of acetylene decomposition can be decreased significantly. Growth of amorphous carbon has been observed at a temperature as low as 323 K.[27] This is probably due to the high affinity between the acidic H atoms of acetylene and the electron rich metallic Na. Formation of NaC≡CH, NaC≡CNa, and NaH as relatively stable intermediates in the process has been proposed.[27,28] Further decomposition of the acetylides and the hydride would produce carbon and hydrogen, while regenerating the active metallic Na to complete the catalytic cycle. We expect that K, a more active alkali metal than Na, would perform analogously through a KC≡CH intermediate.[29] While using alkali metals as the catalysts for growing carbon materials is less reported, many transition metals are frequently employed for that purpose. Among them, Ag has been less explored for the task. This is probably due to its relatively inertness toward hydrocarbon decomposition.[30] In this work, we wish to report our discovery that by coupling K and Ag, an efficient cooperative catalytic system can be established to grow CNCs from acetylene *via* a VLS-type pathway at relatively low temperatures. We have found experimental evidence to elucidate why the bi-catalyst system assists the CNC growth. In addition, investigations on electron field emission (EFE) properties and electrochemical surface areas (ESAs) of the CNCs will be discussed to provide basis for future device applications.

RESULTS AND DISCUSSION

In general, Ag NPs were fabricated on Si substrates either by sputtering or by reducing an aqueous solution of $AgNO_3$ and HF.[31] Then, inside a hot-wall vapor deposition reactor (see Figure S1 in the Supporting Information), K was evaporated to deposit a layer of K thin film on the substrates at low pressure. After acetylene was passed into the reactor at 723 K, 1 atm, deposition of a black thin layer on the substrates was observed. The substrates were removed from the reactor for further characterizations. Upon exposure to air, the residual K metal on the substrates was hydrolyzed. The presence of potassium oxides was observed. Below, we will discuss the characterization and location of the metals and their importance to the CNC growth. Finally, the product was washed with deionized (DI) water to remove the K oxides and left to dry in air. After the washing, the pH value of the water increased from 5.72 to 8.78. The observation was used to estimate the amount of K deposited on the substrate. After several tests, we conclude that the K thicknesses on the substrates were 55−59 nm prior to the CNC growths.

Characterization of Carbon Nanocoils. A scanning electron microscopic (SEM) image of a typical as-grown sample of NCs on Si, after washed by DI water, is shown in Figure 1A. Coil diameters of the NCs are estimated to be 100−300 nm. Pitches (distances between adjacent coils) of the NCs also differ widely. In the inset, a high magnification SEM image reveals a discerned NP at the tip of a NC. In the transmission electron microscopic (TEM) studies discussed below, a similar NP is observed and characterized to be Ag by energy dispersive X-ray spectra (EDS). Figure 1B displays the side-view image of

the sample. It reveals that the overall thickness of the NC layer is about 20 μm. The EDS analysis shown in Figure 1C indicates that C is the major constituent in the sample. Thus, the NCs are determined conclusively to be a carbon-based material. Effect of growth time on the CNC length is shown in Figure 1D using the data displayed in Figure S2 in the Supporting Information. We found that no CNCs were grown on the Si substrate at 5 min. When the reaction was carried out for 10 min, short CNCs with an averaged length of 6.5 μm (calcd from 50 CNCs) were obtained. The averaged CNC length increased significantly to 21.5 and 75.4 μm after the reaction time was extended to 15 and 60 min, respectively. The observations suggest that the reaction required some initiation at the beginning. On the other hand, the presence of densely populated fast-grown CNCs on the substrates suggests that the current deposition was an effective process. An as-grown CNC sample was further heat-treated at 1423 K for 2 h. As shown in Figure 1E, its overall coil morphology does not change. In Figure 1F, Raman spectra of an as-grown CNC sample before and after the annealing are shown. The as-grown sample reveals two relatively broad and overlapping peaks at 1345 and 1588 cm^{-1}, assigned to the D band and the G band of carbon materials, respectively.[32] Shapes of the peaks suggest that the as-grown CNCs are composed of disordered carbon with a low degree of graphitization. On the other hand, the annealed sample shows its D and G band peaks at 1337 and 1583 cm^{-1}, respectively. Compared to those of the as-grown CNCs, the annealed CNCs display well-separated high intensity peaks. The G band position shifts toward that of a pyrolytic graphite sample (1581 cm^{-1}).[33] Furthermore, the I_D/I_G value decreases from 2.64 to 2.03 after the heat treatment. These suggest that the degree of orderness of the annealed sample is higher than the as-grown one.[34] This is further confirmed by the ED studies described below.

TEM studies of a typical as-grown CNC are shown in Figure 2. The low magnification image, Figure 2A, indicates that the CNC has a wire structure (diameter *ca.* 80 nm) with a coil pitch of 100 nm and a coil diameter of 200 nm. Its body is composed of amorphous carbon, as indicated by the electron diffraction (ED) pattern (inset Figure 2A) and the EDS result (Figure 2B). The CNC tip is further enlarged and shown in Figure 2C. A NP with a diameter of about 50 nm wrapped completely inside the tip is clearly observed. The selected-area ED (SAED) pattern shown in the inset of Figure 2C agrees with the presence of a face-centered-cubic (fcc) structure. The EDS in Figure 2D indicates that, in addition to C, the tip contains a high concentration of Ag, but the K concentration is below the EDS detection limit. On the basis of the observations, we conclude that the NP at the tip is Ag. Its importance to the CNC growth will be discussed below. TEM studies of an annealed CNC were shown in Figure S3 in the Supporting Information. The

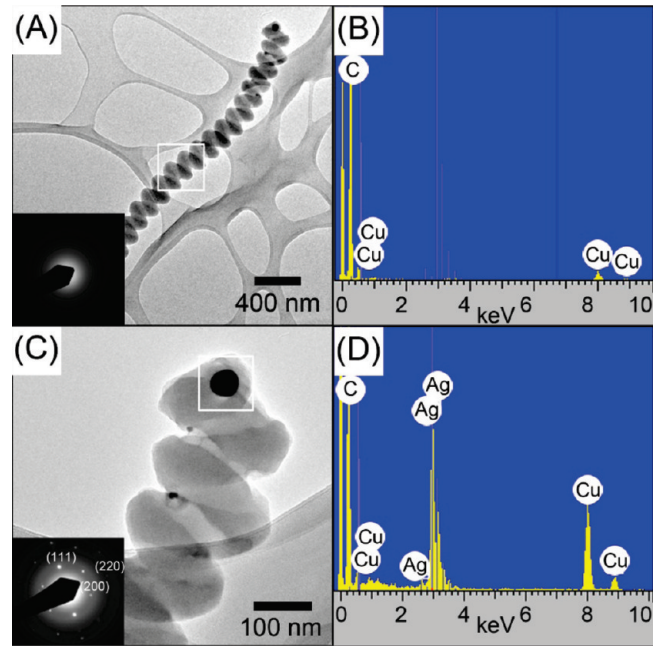

Figure 2. TEM studies of a CNC. (A) Low magnification image and ED pattern from the squared region (inset), (B) EDS from the squared region in (A), (C) high magnification image and ED from the squared region (inset) of the tip, and (D) EDS from the squared region in (C). The signals of Cu in the EDS were from the TEM grid.

low and high magnification images confirmed its coil structure. In a high-resolution transmission electron microscopic (HRTEM) image, from a crystallite with a size of about 3.2 nm, a set of fringes with a lattice spacing value of 0.34 nm was observed and assigned to the distance of graphite (002) planes.[35] The SAED revealed slightly diffused rings. Among them, the two most strong ones were assigned to the reflections from graphite (002) and (004) planes.

To observe the location of metallic K in the sample was more difficult than to find the Ag NPs because K has a much lower melting point, higher volatility, and higher reactivity than Ag. Thus, we converted K in the as-grown samples into more stable K containing products and observed their locations as indicators to the original K positions. We discovered the presence of K oxide particles near the CNC tips by SEM and EDS when the as-grown CNCs were not washed by DI water, as shown in Figure S4 in the Supporting Information. This suggests that K probably coexisted with Ag at the tip during the NC growth. To further confirm the location of K, we carried out the following investigations. After the CNC growth was completed, the reactor temperature was lowered from 723 to 573 K. This reduced the volatility of K by decreasing its vapor pressure inside the reactor (Vapor pressures of K at 573 K, 0.58 Torr, and at 723 K, 16.5 Torr. Estimated using the Clausius−Clapeyron equation with bp of K, 1032 K, and enthalpy of vaporization of K at STP, 76.9 kJ/mol. A thin layer of K atoms could condense on the nanocoil body. Some residual K might exist on the nanocoil surface, also. This is because liquid K, with its low sur-

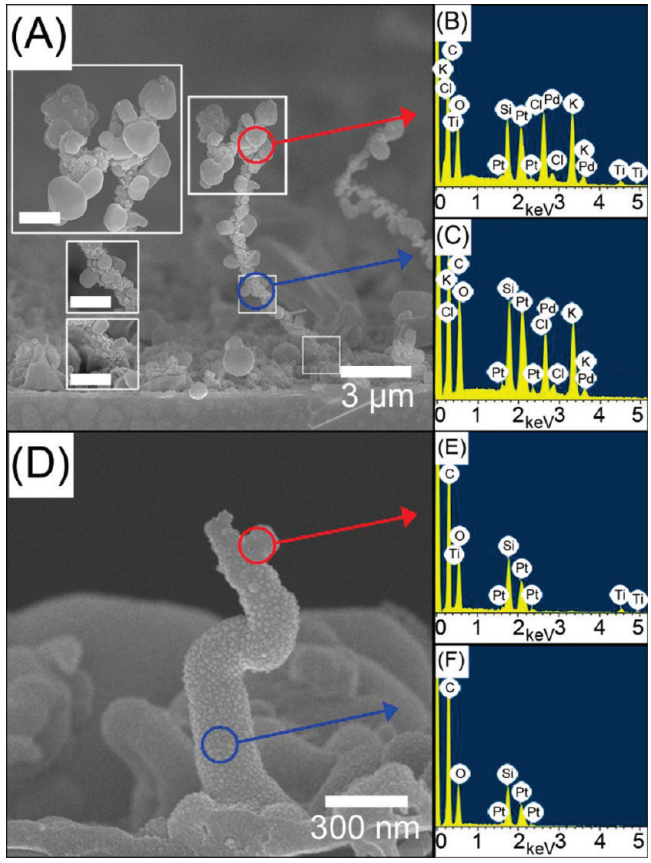

Figure 3. (A) SEM image of $TiCl_4$-treated CNCs. Insets are the magnified views (scale bar: 1 μm) from the squared regions on the right. EDS data of (B) the red-circled and (C) the blue-circled regions in (A). (D) SEM image of a $TiCl_4$-treated CNC after the KCl crystals were removed. EDS data of (B) the red-circled and (C) the blue-circled regions in (D). The Pd and Pt signals in the EDS data were from the sputtered metallic layer for increasing conductivity. The Si signal was from the substrate. The O signal was from the surface oxidation.

face tension among the metals, can wet carbon surface effectively.[36−38]) Then, we passed vapor phase $TiCl_4$ into the reactor to "fix" K into stable solid products containing KCl and Ti for identification. Their positions should indicate the K location upon the completion of the CNC growth. In the X-ray diffraction (XRD) pattern displayed in Figure S5 in the Supporting Information, the $TiCl_4$-treated sample showed the reflections of KCl. As shown in the SEM image in Figure 3A, many solid particles are found on the CNCs, especially at their tips. The EDS signals of Ti atoms are observed at the tip, as shown in Figure 3B. Also, clusters of KCl crystals can be observed in the same region. These data agree with the potassium oxide location observed in Figure S4. All of them suggest that the major positions of K were at the tips of the CNCs upon the completion of the growth. Nonetheless, as suggested by the EDS in Figure 3C, some KCl crystals can be found along the CNC body shown in Figure 3A. As mentioned above, a trace of K might still exist on the coil body prior to the introduction of $TiCl_4$. This is due to the condensation of K and its ability to wet carbon surface. Consequently, after $TiCl_4$ was introduced, KCl particles formed on the coil body, too. Because the quantity of deposited Ti was only a quarter of that of KCl (based on the fact that the reaction stoichiometry between $TiCl_4$ and K is 1 to 4), the EDS signals of Ti from the coil body (Figure 3C) are negligible. After the KCl crystals were removed from the CNCs by evaporation at 1073 K under vacuum, exposed coils were obtained. As shown by the example in Figure 3D, a small particle is found at the tip of the CNC. The EDS study in Figure 3E suggests that the particle contains Ti. The Ti content on the body of the coil is below the detection limit of EDS (Figure 3F). Thus, we conclude that both K and Ag metals located at the tips of the CNCs after the growth. This implies that, during the growth, the metal particles coexisted at the tips of the elongating nanocoils. It is known that Ag and K do not form stable intermetallic phases under normal conditions.[39] Accordingly, we suggest that Ag and K did not form an alloy particle during the CNC growth and the deposition was *via* a VLS-type tip-growth mechanism employing both metals as the catalysts.

Effects of Growth Parameters on Carbon Nanocoil Formation. To understand more about the reaction, we have changed the reaction conditions to observe how these would affect the CNC growth. Our findings are described below. To verify the importance of the copresence of K and Ag in the reaction, we deposited three different metal compositions on a Si substrate. Three zones were K-only, K and Ag, and Ag-only. After the reaction was carried out, we discovered that CNCs were grown only on the surface with both K and Ag, as shown in Figure S6 in the Supporting Information. On the K-only surface, a carbon film was deposited as the only product. On the Ag-only surface, little carbon was deposited. The observation suggests the necessity of both K and Ag in the process. They functioned cooperatively to assist the catalytic growth of CNCs. The density of Ag NPs also played an important role in the reaction. As shown in Figure S7 in the Supporting Information, the density of CNCs grown on a Si surface decreased as the density of Ag NPs was reduced. The result indicates that the Ag NPs probably worked as the seeds for the CNC growth even though the metal could not assist acetylene decomposition effectively. We also performed a preliminary study to show that Au NPs could be applied as the seeds and worked together with K to grow CNCs from acetylene under analogous conditions. Successful growth of amorphous CNCs was confirmed by the data shown in Figure S8 in the Supporting Information. Presence of an Au NP at the tip of a CNC was also observed.

Furthermore, we discovered that the CNCs could be grown efficiently only within a certain temperature range. In Figure S9 in the Supporting Information, it showed that 723 K was the best temperature to grow high density CNCs on Si. Relatively short CNCs were grown at 623 K, while a thick carbon film with limited number of CNCs was the major product deposited at

773 K. We also found that the CNCs could be grown effectively only under a certain combination of acetylene and carrier gases. In Figure S10 in the Supporting Information, it revealed that a mixture of 3 sccm of acetylene and 20 sccm of H_2 provided the best growth of CNCs. In another case, wormlike carbon products were obtained when Ar, instead of H_2, was used as the carrier gas. Another example showed that relatively short CNCs were deposited when the flow rate of acetylene was increased, while the flow rate of H_2 was kept the same. The observations could be rationalized by how H atoms, generated in the decomposition of acetylene, passivated the surface of liquid phase K catalyst. In the case of using Ar as the carrier gas, the main gas stream was H_2-deficient. More H atoms would desorb from the K surface in the form of H_2 molecules. Consequently, the surface was less covered by H atoms. The as-deposited C solid would adhere well to the surface to form the observed morphology. On the other hand, when the flow rate of acetylene was increased, there would be more H atoms, dissociated from acetylene molecules, to occupy the reactive sites on the K surface. As a result, the rate of carbon growth was decreased because fewer surface sites were available to facilitate the acetylene decomposition.

Proposed Reaction Pathway. From the experimental results discussed above, we have found that the CNCs can only be grown when some certain sets of reaction parameters were properly applied. The copresence of both K and Ag particles on the Si surface was the most important factor for the growth. Without Ag, a carbon thin film was still deposited but CNCs could not be grown. Without K, the reaction ceased with little carbon deposition. In successful CNC growths, the presence of both metals at the tips of the coils was determined experimentally. On the basis of the above information, we propose a cooperative bimetal catalyst enhanced tip-growth VLS mechanism in Scheme 1 to elucidate the CNC formation. In the scheme, a catalytic cycle is shown to explain how K assists the acetylene decomposition. In the cycle, C_2H_2 reacts with K exothermically at a relatively low temperature to generate surface intermediates [K]-C≡CH, [K]-C≡C-[K], and [K]-H ([K] denotes a surface K atom). Then, they decompose into *a*-C and H_2, while K is recycled back to the active surface metal atom. It is known that Ag and K do not form alloys, while Ag and C do not dissolve each other well.[39,40] Thus, we suggest that the Ag NP, existing on the liquid phase K particle, acts as the seed for the growth of *a*-C. On the K surface, the as-formed C atoms probably migrate freely until they bind to the Ag NP and extend one-dimensionally (1D) into a nanowire (NW). As the reaction proceeds, more C atoms are produced through the cycle to lengthen the NW. The observed size of the Ag NP, about 50 nm, was much smaller than the measured coil diameter, about 200 nm. This indicates that the Ag NP could not be responsible for the growth of the coil into the observed diameter. Consequently, we propose that K, in addition to assisting acetylene decomposition, probably acts as a template to facilitate the coil formation. We suggest that the growing 1D NW curls along the C−K interface. This is the result of the adhesive force between the liquid phase K particle and the carbon material. It is known that K binds to the carbon well. For example, due to its low surface tension, liquid phase K can wet CNTs effectively.[37,38] In addition, K can intercalate various carbon materials, including glassy carbon, graphite, carbon nanofiber, and fullerenes.[41−45] Many examples of growing CNCs using bicatalysts are summarized in Table S1 in the Supporting Information.[3,18,46] Various possible mechanisms have been proposed to explain how CNCs are formed. The reaction pathway proposed in Scheme 1 in this report provides a new type of CNC growth mechanism.

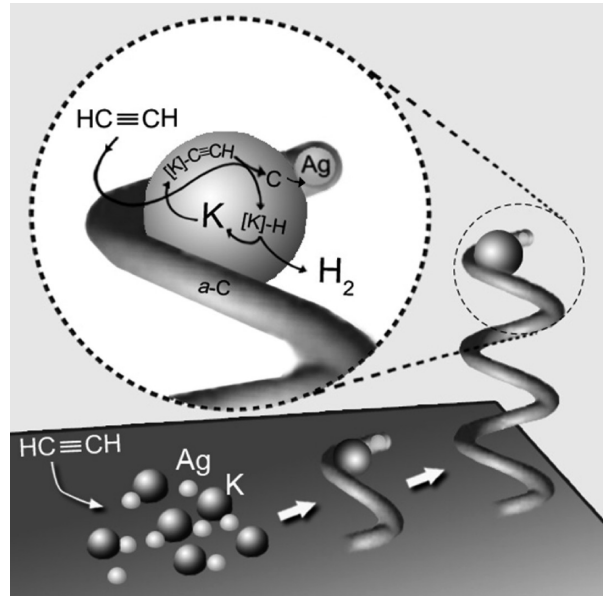

Scheme 1. Proposed CNC growth pathway.

Electron Field Emission Properties of CNCs. The EFE *J*−*E* curves (*J*, current density; *E*, applied field), shown in Figure 4, display the relationship between the emission-current density and the applied field of several CNC samples. The turn-on fields (E_{to}) of the CNCs, determined at a current density of 10 μA/cm^2, were 4.79, 3.24, and 2.80 V/μm for the samples grown for 10, 15, and 60 min, respectively. These values are comparable with the results of CNTs, E_{to} = 1.5−4.5 V/μm[47,48] and consistent with the fact that high aspect ratio CNCs frequently showed low E_{to}.[49] Thus, the emission-current density of the CNCs grown for 60 min reaches 12.22 mA/cm^2 at 5.64 V/μm. Heat treatment could improve the conductivity of CNCs by increasing their crystallinity.[50] As a result, E_{to} of the CNCs grown for 60 min decreases from 2.80 to 2.51 V/μm and *J* increases from 12.22 to 17.71 mA/cm^2 at 5.64 V/μm after the processing. The emission characteristics of the CNCs were fur-

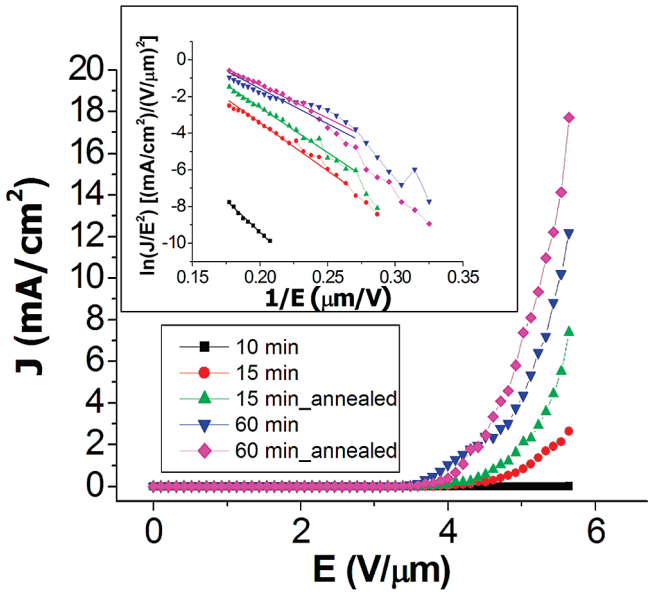

Figure 4. Emission current density as a function of applied electric field on CNC samples. Inset shows their corresponding FN plots.

ther analyzed using Fowler−Nordheim (FN) theory. According to the theory, the relationship between J and E can be described as follows:[51] $J = A(\beta^2E^2/\phi)\exp(-B\phi^{3/2}/\beta E)$, where ϕ is the work function, β is the field enhancement factor, constant A is 1.57×10^{-6} A eV/V^2, and constant B is 6.83 V/(eV$^{3/2}$ nm). From the slopes of the FN plots shown in the inset of Figure 4, we work out the β values by assuming that ϕ of the CNCs is 5 eV.[47] For the samples grown for 10 and 15 min, β are 1112 and 1455, respectively. For the CNCs grown for 60 min, the FN plot shows two slopes corresponding to two β values 1128 and 2010, in the low and the high electric field regions, respectively. This deviation from the FN behavior may be rationalized by the detachment of adsorbates and the interaction between the neighboring tips.[52,53] For the annealed CNC samples grown for 15 and 60 min, β are 1551 and 2124. In addition to their high aspect ratios, the coiled morphology of CNCs might also contribute greatly to the EFE because coiled sides may also function as emitting tips.[54] The calculated β values of the CNCs grown in this study are comparable with the previously reported values summarized in Table S2 in the Supporting Information. These are in the range 600−5000 for CNTs and 200−6000 for CNCs.[8,9,55] We anticipate that the CNCs may find potential applications in field emission-based devices. For example, CNTs have been applied as emitters in a high brightness field-emission display.[56] Recently, a flexible transparent side-electron emission device fabricated from carbon nanofiber has been reported.[57]

Electrochemical Surface Areas of CNCs. Electrochemical behaviors of an electrode (geometric surface area: 0.078 cm^2) fabricated from the annealed CNCs grown for 15 min at 723 K were characterized in an aqueous solution of $K_3[Fe(CN)_6]$ by cyclic voltammetric (CV). Figure 5 shows its current density response to the applied voltage. The result is much stronger than the response of a screen-printed carbon (SPC) electrode (geometric surface area: 0.018 cm^2) used as a reference. CV experiments of ferricyanide performed at different scan rates are frequently employed to estimate ESAs of electrodes using the Randle−Sevcik equation $I_p = 2.69 \times 10^5 AD_0^{1/2}n^{3/2}C_0v^{1/2}$.[58] In the equation, I_p is the reduction peak current, A is the ESA of the electrode, D_0 is the diffusion coefficient of ferricyanide (6.67×10^{-6} cm^2/s),[59] n is the number of electrons transferred in the reaction equation, C_0 is the concentration of ferricyanide in the bulk solution, and v is the scan rate. For the CNC electrode, the CVs obtained at different v were shown in Figure S10 in the Supporting Information. Well-defined voltammetric responses were observed at a potential range −0.2−0.6 V. The peak separation remained a reasonable constant 92 mV at low scan rates 10−60 mV/s, indicating a quasi-reversible process of ferricyanide on the CNC electrode. The peak separation increased slightly from 92 to 133, as v was increased from 60 to 200 mV/s. Similar results were also observed for other carbon material based electrodes.[60] The inset of Figure 5 shows calibrated plots of I_p of $K_3[Fe(CN)_6]$ on the electrodes *versus* the square root of v. Both demonstrate excellent linear relationships with correlation coefficients $R = 0.999$ and 0.999 for the CNC and the SPC electrodes, respectively. From the slopes of the plots, the ESA of the CNC electrode is calculated to be 0.143 cm^2, while the ESA of the SPC reference electrode is 0.013 cm^2. The result suggests that the CNC electrode, with its high ESA, could be employed as electrodes for electrochemical applications. For example, an enzymatic glucose biosensor fabricated from nanoyarn CNT fiber has been reported recently.[61]

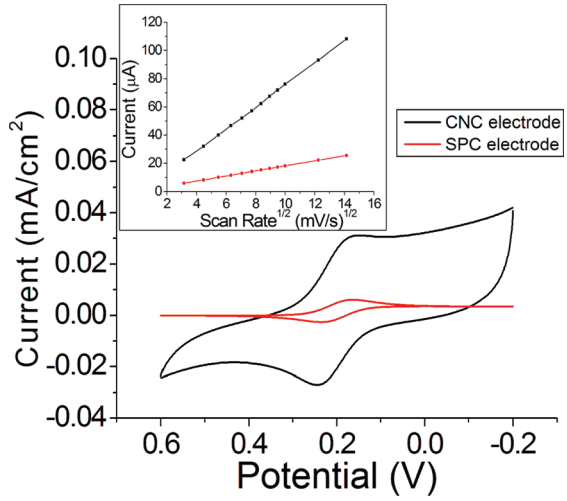

Figure 5. Cyclic voltammograms of CNC (black) and SPC (red) electrodes in an aqueous solution of 2.5 mM $K_3[Fe(CN)_6]$ and 0.1 mM KCl at a scan rate 10 mV/s. Inset shows responses of reduction peak current to square root of scan rate of the electrodes.

CONCLUSION

In summary, we have demonstrated that CNCs can be prepared efficiently by K and Ag assisted cooperative catalytic decomposition of acetylene at a relatively low temperature of 723 K. A catalytic cycle is proposed to rationalize the overall dehydrogenation process. In the cycle, the acidic H atoms of C_2H_2 are removed by electron-rich metallic K to generate surface intermediates KH, KC_2H, and K_2C_2 exothermically. Then, these intermediates decompose into *a*-C and H_2, while K is recycled back to the active metal. Ag NP acts as the active growth site for the nanosized 1D *a*-C NW. Formation of the coiled structure may be attributed to the adhesion between the as-grown 1D *a*-C NW and the surface of the spherical liquid droplet of K. This bends the NW along the surface curvature of the K droplet. The overall growth is a VLS type tip-growth process. Our observation provides a new CNC growth mechanism. The CNCs showed excellent EFE properties. The best sample annealed at 1423 K emitted electrons (10 $\mu A/cm^2$) at E_{to} of 2.51 V/μm, while J_{max} reached 17.71 mA/cm^2 at 5.64 V/μm. The field enhancement factor β was calculated to be 2124, comparable to many other CNT and CNC based emitters. The performance is probably due to the coiled morphology, which allows the electrons to emit not only from the tip but also from the coiled body. In addition, the CNCs showed a high estimated ESA value of 0.143 cm^2, which is much higher than its geometric surface area, 0.078 cm^2. Thus, the process reported in this study is capable of growing CNCs as promising electrodes for both future EFE and electrochemical device applications.

EXPERIMENTAL SECTION

Growth of Carbon Nanocoils. A better set of growth conditions was identified after the reaction parameters were changed in several experiments. These conditions are described below as a general procedure. Ag NPs were fabricated on cleaned *n*-Si(100) substrates (1 $\times$ 1 cm^2) by sputtering or by reducing a solution of $AgNO_3$ (0.1−4 mM, Shimakyu's Pure Chemical 99%, *Caution*: corrosive) and HF (0.552 M, Merck 48%, *Caution*: toxic and corrosive). The substrates were put in a 10 cm quartz boat placed at 30 cm downstream from the center of a hot-wall reactor. The reactor was composed of a Lindberg HTF55122A tube furnace and a 27 mm diameter quartz tube (Figure S1). Another quartz boat loaded with KH powder (0.15 g, 3.7 mmol, Aldrich 30% in mineral oil, *Caution*: highly flammable and corrosive) was placed at the center of the reactor. KH was thermally decomposed to form liquid K at 623 K under 1 atm of Ar (flow rate: 20 sccm) for 1 h. The K liquid was evaporated at 2 $\times$ 10^{-3} Torr, 423 K, for 30 min to deposit a layer of K thin film on the substrates at 353 K. Then, the K-coated Si substrates were pulled to the center of the furnace under Ar (1 atm). Acetylene (3 sccm) was carried into the reactor by a flow of H_2 (20 sccm) at 723 K for 15 min. After the apparatus was cooled down to room temperature, deposition of a black thin layer on the substrate was observed. The product was removed from the reactor and exposed to air so that the residual K metal was hydrolyzed. Finally, the product was washed with DI water to remove the K oxides and left to dry in air. Some of the CNC samples were further heat-treated at 1423 K in 1 atm of Ar (flow rate: 20 sccm) for 2 h.

To estimate the amount of K deposited on a substrate, the following experiment was carried out. A Si substrate (1 $\times$ 0.5 cm^2) was used to grow CNCs using the steps discussed above. Then, the substrate with the as-deposited CNCs was placed in DI water (10 mL) to dissolve the K oxides. The pH value of the solution increased from 5.72 to 8.78. By assuming that the hydroxide concentration increase equaled the amount of K ions dissolved in the solution, the quantity of K deposited on the substrate was estimated to be 2.35 $\times$ 10^{-3} mg (6.02 $\times$ 10^{-5} mmole). When the atomic weight and the molar volume of K was 39.09 g/mol and 45.94 cm^3/mol, respectively, the K thickness on the substrate was determined to be 55 nm. Another estimation for the K layer on another Si substrate showed that the thickness was 59 nm.

The location of K metal on the sample was studied using the following process. After the CNCs were grown, $TiCl_4$ was introduced into the reactor at 1 atm, 573 K, by using Ar (20 sccm) as the carrier gas for 1 h. Distribution of KCl crystals on the sample was observed. The position of Ti atoms was determined after the KCl crystals were evaporated under vacuum at 1073 K. Both the locations of Ti and KCl were used to determine that K located at the tips of nanocoils during the growth.

Instruments for Characterizations. SEM images and EDS of the samples were taken with a Hitachi S-4000 and a JEOL JSM-7401F operated at 15 keV. TEM, ED, HRTEM images, and EDS were acquired on a JEOL JEM-3000F at 300 kV and a JEOL JSM-2010 at 200 kV. XRD patterns of the samples were obtained using a Bruker AXS D8 Advance with Cu Kα1 radiation. Raman spectra were measured by a high resolution confocal Raman microscope (Horiba, LabRAM HR) with an excitation wavelength of 532 nm. A Eutech Instruments CyberScan pH510 was used to measure the pH value.

Electron Field Emission Property Measurements. EFE properties of the CNCs were carried out in a vacuum chamber with a base pressure of 2 $\times$ 10^{-6} Torr. A spherical-shaped tungsten tip with a diameter of 1 mm was used as the anode, while the CNCs on Si substrates were placed on the sample stage and used as the cathode. The gap between the anode and the CNCs was maintained at 195 μm. The field emission currents were measured with a Keithley 2410 High Voltage SourceMeter (0−1100 V, with an increment of 20 V).

Electrochemical Surface Area Measurements. The heat-treated CNCs on Si substrates were used as the working electrodes directly. SPC electrodes (Zensor, diameter: 1.5 mm) were used for comparison. Electrochemical measurements in a three-electrode system were carried out using an electrochemical analyzer (CH Instruments 6081C). A Pt wire was used as the counterelectrode, while an Ag|AgCl electrode was used as the reference electrode. All potentials were quoted relative to the Ag|AgCl reference. Before the measurements were carried out, the electrodes were cleaned with ethanol and water and then left to dry in air. Electron-transfer properties of the electrodes were evaluated by using CV studies carried out in a solution (20 mL) containing KCl (0.1 mM) and $K_3[Fe(CN)_6]$ (2.5 mM). ESAs of the electrodes were calculated from the corresponding currents of the voltammetric peaks, in accordance with the Randle−Sevcik equation.[58]

Acknowledgment. We are grateful for the support from the National Science Council, "Aim for the Top University Plan" of the National Chiao Tung University, and the Ministry of Education of Taiwan, the Republic of China. Also, we thank Mr. Tsung-Yu Tsou for assisting EFE sample preparations.

Supporting Information Available: Tables of literature summaries, experimental setup of the CVD system, SEM and TEM images, EDS data, ED and XRD patterns, and CV diagrams. This material is available free of charge *via* the Internet at http://pubs.acs.org.

REFERENCES AND NOTES

1. Iijima, S. Helical Microtubules of Graphitic Carbon. *Nature* **1991**, *354*, 56–58.

2. Wen, Y. K.; Shen, Z. M. Synthesis of Regular Coiled Carbon Nanotubes by Ni-Catalyzed Pyrolysis of Acetylene and a Growth Mechanism Analysis. *Carbon* **2001**, *39*, 2369–2374.
3. Wang, W.; Yang, K. Q.; Gaillard, J.; Bandaru, P. R.; Rao, A. M. Rational Synthesis of Helically Coiled Carbon Nanowires and Nanotubes Through the Use of Tin and Indium Catalysts. *Adv. Mater.* **2008**, *20*, 179–182.
4. Qin, Y.; Jiang, X.; Cui, Z. Low-Temperature Synthesis of Amorphous Carbon Nanocoils *via* Acetylene Coupling on Copper Nanocrystal Surfaces at 468 K: A Reaction Mechanism Analysis. *J. Phys. Chem. B* **2005**, *109*, 21749–21754.
5. Bajpai, V.; Dai, L. M.; Ohashi, T. Large-Scale Synthesis of Perpendicularly Aligned Helical Carbon Nanotubes. *J. Am. Chem. Soc.* **2004**, *126*, 5070–5071.
6. Chang, N.-K.; Chang, S.-H. High-Yield Synthesis of Carbon Nanocoils on Stainless Steel. *Carbon* **2008**, *46*, 1106–1109.
7. Tang, N.; Zhong, W.; Au, C.; Yang, Y.; Han, M.; Lin, K.; Du, Y. Synthesis, Microwave Electromagnetic, and Microwave Absorption Properties of Twin Carbon Nanocoils. *J. Phys. Chem. C* **2008**, *112*, 19316–19323.
8. Pan, L. J.; Hayashida, T.; Zhang, M.; Nakayama, Y. Field Emission Properties of Carbon Tubule Nanocoils. *Jpn. J. Appl. Phys.* **2001**, *40*, L235–L237.
9. Sung, W. Y.; Ok, J. G.; Kim, W. J.; Lee, S. M.; Yeon, S. C.; Lee, H. Y.; Kim, Y. H. Synthesis and Field Emission Characteristics of Carbon Nanocoils with a High Aspect Ratio Supported by Copper Micro-Tips. *Nanotechnology* **2007**, *18*, 245603 - 1−5.
10. Chen, X.; Zhang, S.; Dikin, D. A.; Ding, W.; Ruoff, R. S.; Pan, L.; Nakayama, Y. Mechanics of a Carbon Nanocoil. *Nano Lett.* **2003**, *3*, 1299–1304.
11. Daraio, C.; Nesterenko, V. F.; Jin, S.; Wang, W.; Rao, A. M. Impact Response by a Foamlike Forest of Coiled Carbon Nanotubes. *J. Appl. Phys.* **2006**, *100*, 064309 - 064309−4.
12. Castrucci, P.; Scarselli, M.; De Crescenzi, M.; El Khakani, M. A.; Rosei, F.; Braidy, N.; Yi, J. H. Effect of Coiling on the Electronic Properties Along Single-Wall Carbon Nanotubes. *Appl. Phys. Lett.* **2004**, *85*, 3857–3859.
13. Chiu, H.-S.; Lin, P.-I.; Wu, H.-C.; Hsieh, W.-H.; Chen, C.-D.; Chen, Y.-T. Electron Hopping Conduction in Highly Disordered Carbon Coils. *Carbon* **2009**, *47*, 1761–1769.
14. Hou, H. Q.; Jun, Z.; Weller, F.; Greiner, A. Large-Scale Synthesis and Characterization of Helically Coiled Carbon Nanotubes by Use of $Fe(CO)_5$ as Floating Catalyst Precursor. *Chem. Mater.* **2003**, *15*, 3170–3175.
15. Xie, J. N.; Varadan, V. K. Synthesis of High Yield Single Helical Carbon Microsprings by Catalytic Chemical Vapor Deposition and an Experimental Investigation of Their Growth Mechanism. *J. Appl. Phys.* **2007**, *101*, 114903 - 114903−7.
16. Liu, Q.; Cui, Z.-M.; Ma, Z.; Bian, S.-W.; Song, W.-G. Carbon Materials with Unusual Morphologies and Their Formation Mechanism. *J. Phys. Chem. C* **2007**, *111*, 12420–12424.
17. Kuzuya, C.; In-Hwang, W.; Hirako, S.; Hishikawa, Y.; Motojima, S. Preparation, Morphology, and Growth Mechanism of Carbon Nanocoils. *Chem. Vap. Deposition* **2002**, *8*, 57–62.
18. Okazaki, N.; Hosokawa, S.; Goto, T.; Nakayama, Y. Synthesis of Carbon Tubule Nanocoils Using Fe-In-Sn-O Fine Particles as Catalysts. *J. Phys. Chem. B* **2005**, *109*, 17366–17371.
19. Chen, X. Q.; Saito, T.; Kusunoki, M.; Motojima, S. Three-Dimensional Vapor Growth Mechanism of Carbon Microcoils. *J. Mater. Res.* **1999**, *14*, 4329–4336.
20. Amelinckx, S.; Zhang, X. B.; Bernaerts, D.; Zhang, X. F.; Ivanov, V.; Nagy, J. B. A Formation Mechanism for Catalytically Grown Helix-Shaped Graphite Nanotubes. *Science* **1994**, *265*, 635–639.
21. Pan, L.; Zhang, M.; Nakayama, Y. Growth Mechanism of Carbon Nanocoils. *J. Appl. Phys.* **2002**, *91*, 10058–10061.
22. Bandaru, P. R.; Daraio, C.; Yang, K.; Rao, A. M. A Plausible Mechanism for the Evolution of Helical Forms in Nanostructure Growth. *J. Appl. Phys.* **2007**, *101*, 094307 - 094307−4.
23. Wang, L.-S.; Lee, C.-Y.; Chiu, H.-T. New Nanotube Synthesis Strategy—Application of Sodium Nanotubes Formed Inside Anodic Aluminium Oxide as a Reactive Template. *Chem. Commun.* **2003**, 1964–1965.
24. CRCT, École Polytechnique de Montréal, Facility for the Analysis of Chemical Thermodynamics. http://www.crct.polymtl.ca/fact/ (Reaction-Web).
25. Weast, R. C., Ed. *CRC Handbook of Chemistry and Physics*, 58th ed.; CRC Press: West Palm Beach, FL, 1977−78; F231.
26. Bretherick, L. *Hazards in the Chemical Laboratory*; The Royal Society of Chemistry: London, 1986.
27. Wang, L.-S. Ph.D. Thesis, National Chiao Tung University, 2006.
28. Addison, C. C.; Hobdell, M. R.; Pulham, R. J. The Reactions of Acetylene and Propyne at the Surface of Liquid Sodium. *J. Chem. Soc. A* **1971**, 1704–1708.
29. Xin, J.; Ziurys, L. M. The Submillimeter-Wave Spectrum of KCCH ($X1\Sigma$). *Astrophys. J. Lett.* **1998**, *501*, L151–L153.
30. Takagi, D.; Homma, Y.; Hibino, H.; Suzuki, S.; Kobayashi, Y. Single-Walled Carbon Nanotube Growth from Highly Activated Metal Nanoparticles. *Nano Lett.* **2006**, *6*, 2642–2645.
31. Peng, K.-Q.; Yan, Y.-J.; Gao, S.-P.; Zhu, J. Synthesis of Large-Area Silicon Nanowire Arrays *via* Self-Assembling Nanoelectrochemistry. *Adv. Mater.* **2002**, *14*, 1164–1167.
32. Wang, L.-S.; Wang, C.-H.; Peng, C.-W.; Lee, C.-Y.; Chiu, H.-T. Elongation of Arrays of Amorphous Carbon Tubes. *Carbon* **2005**, *43*, 2618–2621.
33. Wilhelm, H.; Lelaurain, M.; McRae, E.; Humbert, B. Raman Spectroscopic Studies on Well-Defined Carbonaceous Materials of Strong Two-Dimensional Character. *J. Appl. Phys.* **1998**, *84*, 6552–6558.
34. Bi, H.; Kou, K.-C.; Ostrikov, K.; Zhang, J.-Q. Graphitization of Nanocrystalline Carbon Microcoils Synthesized by Catalytic Chemical Vapor Deposition. *J. Appl. Phys.* **2008**, *104*, 033510 - 033510−6.
35. International Center for Diffraction Data. *Joint Committee for Powder Diffraction (JCPDS), File No. 75-2078*, **1982**.
36. Weast, R. C., Ed. *CRC Handbook of Chemistry and Physics*, 58th ed.; CRC Press: West Palm Beach, FL, 1977−78; F25−F38.
37. Dujardin, E.; Ebbesen, T. W.; Hiura, H.; Tanigaki, K. Capillarity and Wetting of Carbon Nanotubes. *Science* **1994**, *265*, 1850–1852.
38. Dujardin, E.; Ebbesen, T. W.; Krishnan, A.; Treacy, M. M. J. Wetting of Single Shell Carbon Nanotubes. *Adv. Mater.* **1998**, *10*, 1472–1475.
39. Kienast, G.; Verma, J. The Behavior of Alkali Metals Towards Cu, Ag, and Au. *Z. Anorg. Allg. Chem.* **1961**, *310*, 143–169.
40. Massalski, T. B., Ed. *Binary Alloy Phase Diagrams*, 2nd ed.; The Materials Information Society, ASM International: Materials Park, OH, 1992.
41. Halpin, M. K.; Jenkins, G. M. Interaction of Glassy Carbon with Alkali Metal Vapours. *Proc. R. Soc. London, Ser. A* **1969**, *313*, 421–431.
42. Dresselhaus, M. S.; Dresselhaus, G. Intercalation Compounds of Graphite. *Adv. Phys.* **2002**, *51*, 1–186.
43. Michel, J. A.; Robinson, V. S.; Yang, L.; Sambandam, S.; Lu, W.; Westover, T.; Fisher, T. S.; Lukehart, C. M. Synthesis and Characterization of Potassium Metal/Graphitic Carbon Nanofiber Intercalates. *J. Nanosci. Nanotechnol.* **2008**, *8*, 1942–1950.
44. Haddon, R. C.; Hebard, A. F.; Rosseinsky, M. J.; Murphy, D. W.; Duclos, S. J.; Lyons, K. B.; Miller, B.; Rosamilia, J. M.; Fleming, R. M.; Kortan, A. R.; et al. Conducting Films of C_{60} and C_{70} by Alkali-Metal Doping. *Nature* **1991**, *350*, 320–322.
45. Ossipyan, Y. A. Fullerene and Fullerites - New Modern Materials. *J. Phys. IV* **1994**, *4*, 51–73.
46. Kanada, R.; Pan, L.; Akita, S.; Okazaki, N.; Hirahara, K.; Nakayama, Y. Synthesis of Multiwalled Carbon Nanocoils Using Codeposited Thin Film of Fe−Sn as Catalyst. *Jpn. J. Appl. Phys.* **2008**, *47*, 1949–1951.
47. Bonard, J.-M.; Salvetat, J.-P.; Stöckli, T.; de Heer, W. A.;

Forró, L.; Châtelain, A. Field Emission from Single-Wall Carbon Nanotube Films. *Appl. Phys. Lett.* **1998**, *73*, 918–920.
48. Bonard, J.-M.; Croci, M.; Klinke, C.; Kurt, R.; Noury, O.; Weiss, N. Carbon Nanotube Films as Electron Field Emitters. *Carbon* **2002**, *40*, 1715–1728.
49. Qian, X.; Liu, H.; Guo, Y.; Song, Y.; Li, Y. Effect of Aspect Ratio on Field Emission Properties of ZnO Nanorod Arrays. *Nanoscale Res. Lett.* **2008**, *3*, 303–307.
50. Zeng, B.; Xiong, G.; Chen, S.; Wang, W. Z.; Wang, D. Z.; Ren, Z. F. Enhancement of Field Emission of Aligned Carbon Nanotubes by Thermal Oxidation. *Appl. Phys. Lett.* **2006**, *89*, 223119223119−3.
51. Fowler, R. H.; Nordheim, L. W. Electron Emission in Intense Electric Fields. *Proc. R. Soc. London, Ser. A* **1928**, *119*, 173–181.
52. Dean, K. A.; Chalamala, B. R. Current Saturation Mechanisms in Carbon Nanotube Field Emitters. *Appl. Phys. Lett.* **2000**, *76*, 375–377.
53. Collins, P. G.; Zettl, A. Unique Characteristics of Cold Cathode Carbon-Nanotube-Matrix Field Emitters. *Phys. Rev. B* **1997**, *55*, 9391–9399.
54. Pan, L.; Konishi, O.; Tanaka, H.; Suekane, O.; Nosaka, T.; Nakayama, Y. Effect of Morphology on Field Emission Properties of Carbon Nanocoils and Carbon Nanotubes. *Jpn. J. Appl. Phys.* **2005**, *44*, 1652–1654.
55. Choi, J. H.; Choi, S. H.; Han, J.-H.; Yoo, J.-B.; Park, C.-Y.; Jung, T.; Yu, S.-G.; Han, I.-T.; Kim, J. M. Enhanced Electron Emission from Carbon Nanotubes Through Density Control Using In Situ Plasma Treatment of Catalyst Metal. *J. Appl. Phys.* **2003**, *94*, 487–490.
56. Choi, W. B.; Chung, D. S.; Kang, J. H.; Kim, H. Y.; Jin, Y. W.; Han, I. T.; Lee, Y. H.; Jung, J. E.; Lee, N. S.; Park, G. S.; et al. Fully Sealed, High-Brightness Carbon-Nanotube Field-Emission Display. *Appl. Phys. Lett.* **1999**, *75*, 3129–3131.
57. Nakamura, H.; Yanagi, H.; Kita, T.; Magario, A; Noguchi, T. Side Electron Emission Device Using Carbon Nanofiber/Elastomer Composite Sheet. *Appl. Phys. Lett.* **2008**, *92*, 243302−1 - 243302−3.
58. Bard, A. J.; Faulkner, L. *Electrochemical Methods: Fundamentals and Applications*, 2nd ed.; Wiley: New York, 2001.
59. Ohnuki, Y.; Matsuda, H.; Ohsaka, T.; Oyama, N. Permselectivity of Films Prepared by Electrochemical Oxidation of Phenol and Amino-Aromatic Compounds. *J. Electroanal. Chem.* **1983**, *158*, 55–67.
60. Yao, Y.; Shiu, K.-K. Electron-Transfer Properties of Different Carbon Nanotube Materials, and Their Use in Glucose Biosensors. *Anal. Bioanal. Chem.* **2007**, *387*, 303–309.
61. Zhu, Z.; Song, W.; Burugapalli, K.; Moussy, F.; Li, Y.-L.; Zhong, X.-H. Nano-Yarn Carbon Nanotube Fiber Based Enzymatic Glucose Biosensor. *Nanotechnology* **2010**, *21*, 165501-1–165501-10.